Hierarchically Structured Cobalt Oxide (Co_3O_4): The Morphology Control and Its Potential in Sensors

An-Min Cao,[†,§] Jin-Song Hu,[†] Han-Pu Liang,[†] Wei-Guo Song,[†] Li-Jun Wan,*[,†] Xiu-Li He,[‡] Xiao-Guang Gao,[‡] and Shan-Hong Xia[‡]

Beijing National Laboratory for Molecular Science, Institute of Chemistry, Chinese Academy of Sciences (CAS), Beijing 100080, China, Institute of Electronics, Chinese Academy of Sciences (CAS), Beijing 100080, China

Received: May 26, 2006; In Final Form: June 19, 2006

A polyol process was developed to synthesize Co_3O_4 with controllable superstructures. By tuning the reaction conditions, the prepared Co_3O_4 were readily regulated in its morphologies, which could vary from nanosphere to two-dimensional (2D) nanoplates and 3D hierarchical structures, and finally to microspheres. The growth kinetics of such a process was also studied. The synthesized Co_3O_4 exhibited good sensitivity, remarkable selectivity, and high stability as an alcohol sensor material.

Introduction

An unceasing pursuance in materials science and chemistry is to develop materials with better performance, which depend not only on the compositions but also on the morphologies of the materials. The properties of materials with the same composition but different morphologies could be substantially different.[1,2] Scientists have been paying more and more attention to the organization of nanostructures across extended dimensions to design functional materials.[3] The formation of composite structures based on spontaneous processes in which time- and scale-dependent coupling of components generating higher order architectures with embedded substructure is of great interest. As a recently developed concept, the self-assembly technique has been shown to be an efficient "bottom-up" route in fabricating functional materials with different patterns and morphologies.[4,5] It is a spontaneous process, with which complicated organics and hierarchical architecture can be produced. Through intermolecular, intramolecular, and molecule/substrate interactions, various self-assembled monolayers (SAMs) were prepared in two-dimensional (2D) surface.[6−9] However, fabricating three-dimensional (3D) architecture in controllable morphology, orientation, and structure by self-assembly process remains a challenge in the development of nanomaterials and nanodevices.[10,11]

As an important magnetic p-type semiconductor, cobalt oxide (Co_3O_4) is of special interest due to its potential applications as sensors, heterogeneous catalysts, electrochromical devices, and magnetic materials.[12−16] Co_3O_4 with different morphologies such as nanospheres, nanocube, nanofiber, and mesoporous structures have been prepared.[17−20] The properties of the as-synthesized metal oxides strongly depend on their morphologies and structures, including crystal sizes, orientations, stacking manners, aspect ratios and even crystalline densities.[12−22] As far as we know, the systematic research on the morphology evolutions of Co_3O_4 in different dimensions, i.e., from zero dimensional nanospheres to 2D nanoplates, then to 3D hierarchical microspheres, is rarely concerned.

In this paper, a two-step method is adopted to achieve the morphology control of the functional Co_3O_4. In the first step, cobalt acetate reacts with ethylene glycol (EG) in the presence of poly(vinyl pyrrolidone) (PVP) to produce cobalt oxide precursor, and then the precursor is calcinated to produce Co_3O_4. A similar process to form the so-called metal alkoxide has been recently discussed.[23,24] Larcher et al. have studied the reactions between cobalt and different alcohols. These showed that the reaction of Co acetate and EG will lead to nanospheres of Co alkoxide.[23] However, a disk-shaped particle of Co alkoxide was further discovered by Chakroune.[24] A mechanism in which redissolution of the nanospheres to form the disk-shaped particles was then assumed. Intriguingly, in our study, the morphologies of the precursor were greatly varied and such a polyol process was shown to be very complicated. Different crystallization mechanisms were probably involved. Cobalt oxide precursors with various shapes such as nanospheres, nanoplates, semiconvex superstructures, and microspheres could be prepared through delicate control of reaction conditions. A spontaneous morphology transformation from sphere to nanoplate and finally to microspherical architecture is also observed. The calcinated product as Co_3O_4 with special morphology exhibited excellent sensitivity to alcohol vapor, showing its potentials in sensor and related nanodevices.

Experimental Section

In a typical synthesis, $Co(CH_3COO)_2 \cdot 4H_2O$ (Beijing Chemical Reagent Ltd.) and PVP (M_w = 58 000; ACROS Organics) were added to a certain amount of ethylene glycol (Beijing Chemical Reagent Ltd.) to give a cloudy solution. The mixture was stirred with a magnetic stir bar and heated to 170 °C under the protection of argon. The cloudy mixture turned clear in 10 min and became opaque again after 30 min, indicating the formation of cobalt oxide precursor. The products were collected by centrifugation−redispersion cycles with alcohol. This cobalt oxide precursor was calcined at 500 °C for 2 h to obtain crystalline cobalt oxide.

* Address correspondence to this author. Phone and fax: +86-10-62558934. E-mail:wanlijun@iccas.ac.cn.
[†] Institute of Chemistry, Chinese Academy of Sciences.
[§] Also in Graduate School, Chinese Academy of Sciences, Beijing, China.
[‡] Institute of Electronics, Chinese Academy of Sciences.

10.1021/jp0632438 CCC: $33.50
Published on Web 07/26/2006

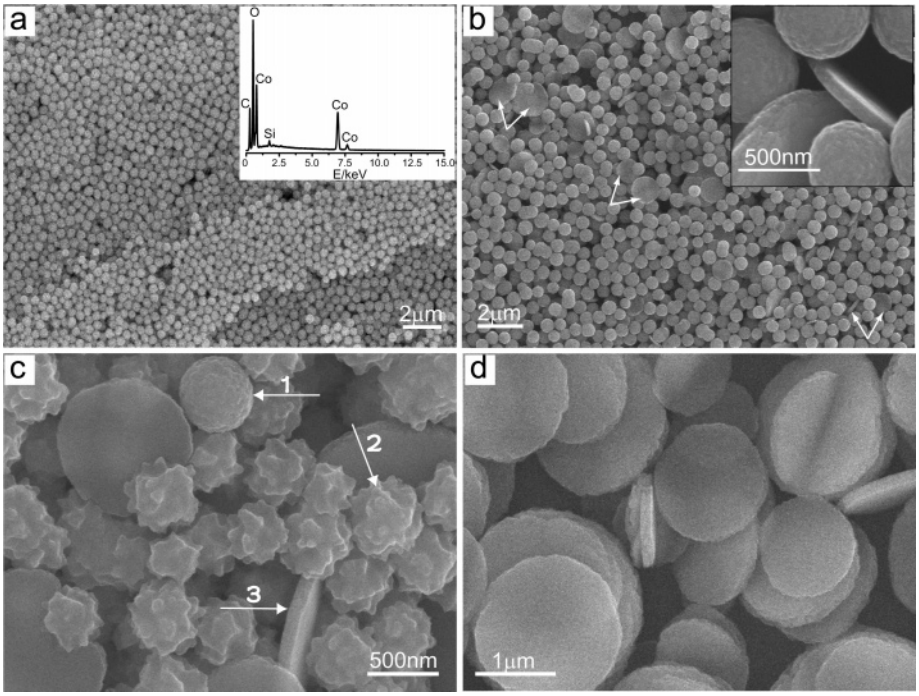

Figure 1. SEM images of the cobalt precursors collected at different stages after the precipitate appeared in clear solution. (a) Sample A, 0 min: the inset is the energy-disperse X-ray (EDX) spectroscopic analysis. (b) Sample B, 10 min: nanoplates are indicated by arrows; the inset shows a high-magnification SEM picture. (c) Sample C, 20 min: the spheres, eroded spheres and nanoplates are labeled respectively. (d) Sample D, 30 min.

The products were characterized by XRD (Rigaku Dmax/rb diffractometer with Cu Kα radiation, $l = 0.1542$ nm, 40 kV, 100 mA), TEM (Philips TECNAI-20), SEM (Hitachi S-4300F), FTIR (Bruker Tensor 27), XPS (ESCALab220I-XL with Al/Mg cathode radiation), and BET (Quantachrome Autosorb Automated Gas Sorption System).

Gas-Sensing Measurement. A silicon wafer was used as substrate, and SiO_2 film was deposited on it for insulating Co_3O_4 from the substrate. A Ta/Pt film was deposited and patterned to act as interdigital electrodes, heater, and temperature senor. All the sensitivity measurements were performed at 300 °C. The sensor was kept in a closed plastic tube equipped with appropriate inlet and outlet. Micromotors were adopted to introduce CO and C_2H_5OH with different concentrations while gas flow could easily be switched between dry air and the sample gas. The conductivities for Co_3O_4 with different morphologies were then measured and its sensitivity is defined as the resistance ratio of R_{gas} to R_o, where R_{gas} and R_o are the electrical resistance for the sensor in C_2H_5OH or CO and in air, respectively.

Results and Discussion

The Morphology Transformation. An EG solution containing 0.23 mM PVP and 9 mM $Co(CH_3COO)_2 \cdot 4H_2O$ was heated at 170 °C for about 30 min under argon protection, which led to the precipitation of cobalt oxide precursors. Time-dependent experiments were conducted to reveal the growth process. The products were collected at different stages from the reaction mixture, and then their morphologies were investigated by SEM.

As shown in Figure 1a, when the cobalt oxide precursors were just precipitated from the clear solution, uniform spheres appeared with a diameter of 500 nm. With different initial $Co(CH_3COO)_2 \cdot 4H_2O$ concentrations, the sphere diameters varied from 100 to 600 nm. Such a sphere shape is consistent with the typical polyol process, in which the precipitates will adopt a spherical shape with minimal surface energy.[25,26] The energy-disperse X-ray (EDX) spectroscopic analysis (inset in Figure 1a) of the spheres indicated the existence of cobalt. From the time-dependent experiments, we found that the as-synthesized spheres ($t = 0$ min, Sample A) gradually changed their morphology during the heating process. After an additional 10 min of reaction, another architecture, round nanoplates, could be observed as indicated by arrows in Figure 1b ($t = 10$ min, Sample B). Its inset showed the details of such morphology. The plates are ca. 2 μm in diameter with a thickness of ca. 90 nm. In the next 10 min, the surfaces of the spheres gradually became rough and small flat terraces appeared as shown in Figure 1c ($t = 20$ min, Sample C), indicating a process of morphology transformation. Several different morphologies can be observed in this period as spheres, eroded spheres, and nanoplates. This is a typical dissolution−renucleation process that results in a gradual erosion and morphology transformation of the spheres. After 30 min the spheres totally disappear and only nanoplates exist in the reaction product as shown in Figure 1d ($t = 30$ min, Sample D).

XRD and FT-IR Characterization. X-ray diffraction (XRD) analysis and Fourier-transfer infrared (FT-IR) spectroscopy were used to investigate the change of composition and structure during the morphologic transformation. Figure 2a showed the XRD results for the above time-dependent experiments. When the product was all spheres as in Sample A, it was amorphous with no apparent peak in the XRD pattern. The emergence of nanoplates indicated the start of the sample crystallization along with the appearance of weak peaks in Sample B. The peak intensities gradually increased while nanoplates replaced spheres, and the precipitation finally turned into highly crystalline cobalt oxide precursor as in Sample D. To determine detailed structure of such a precursor is usually difficult.[23,24] The XRD pattern reported here could be assigned to a layered structure derived form the brucite structure according to Chakroune et al.[24] The main lines in the XRD pattern were indexed as the (00*l*) reflections. It was assumed that the ethylene glycol (EG) would lose its two protons and the dianion complexed with the metal center. Xia et al. has studied the characteristically strong peak

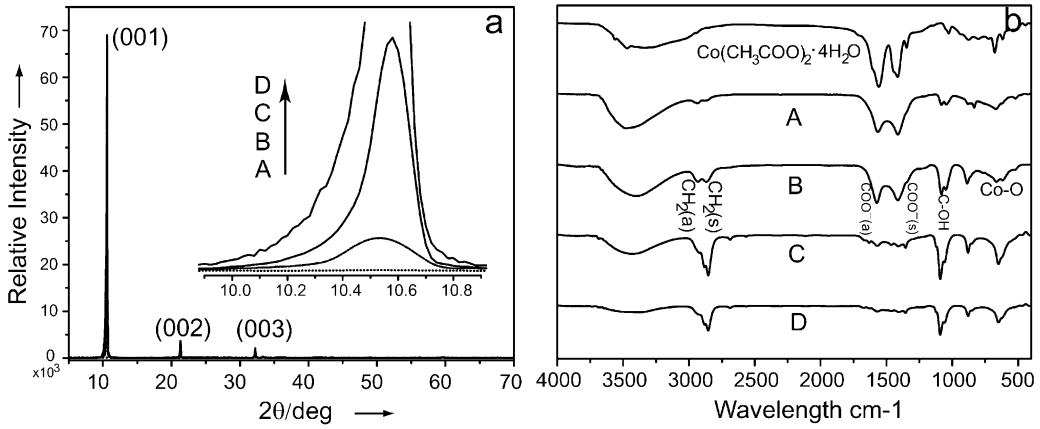

Figure 2. (a) XRD patterns and (b) FT-IR spectra of the precursors from Sample A to Sample D. The inset of panel a is the magnified peak around 10°. For IR spectra, the peaks at 1569 and 1425 cm^{-1} are typical for stretching vibrations of carboxylate group, $\nu_a(COO^-)$ and $\nu_s(COO^-)$, respectively. The peaks at 2882 and 2853 cm^{-1} are ascribed to $\nu_a(CH_2)$ and $\nu_s(CH_2)$, while the strong peak around 1080 cm^{-1} is for C−OH.

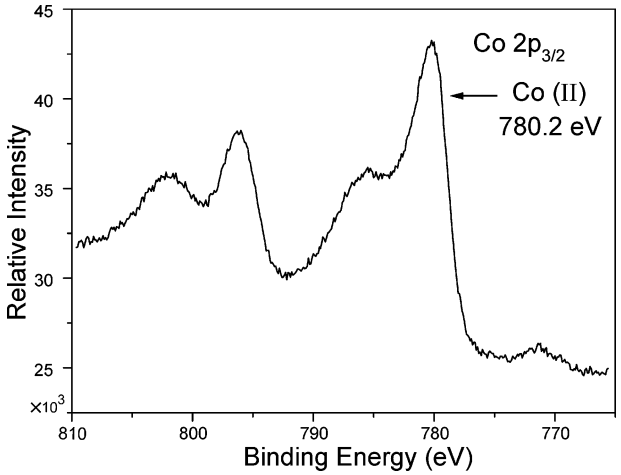

Figure 3. XPS data for Sample D. The Co $2p_{3/2}$ at 780.2 eV and the shake-up peak around 785 eV are typical for pure Co(II) species in the sample.

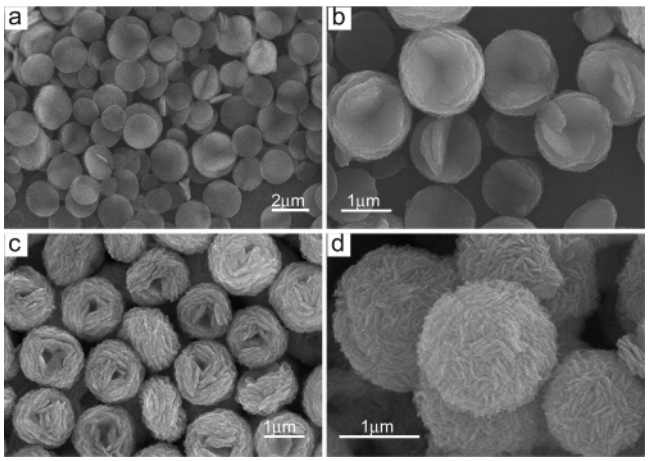

Figure 4. SEM images of the cobalt precursor prepared with different concentrations of $Co(CH_3COO)_2 \cdot 4H_2O$ at (a) 6, (b) 40, (c) 93, and (d) 160 mM while the concentration of PVP was fixed at 0.23 mM.

around 10° in a similar polyol process.[11,27,28] It was considered to be a typical feature from the coordination and alcoholysis of EG with the center metal ions. Such a scheme might also be applicable to the time-dependent process. Figure 2b shows the FT-IR spectra which revealed the gradual replacement of acetate ligands by EG. The intensities of the C−OH vibration band as well as the CH_2− band gradually increased at the expense of the characteristically strong bands of COO− ($Co(CH_3COO)_2 \cdot 4H_2O$). X-ray photoelectron spectroscopy (XPS) studies in Figure 3 indicate that the cobalt exists as cobalt(II) in the nanoplates. Thus the morphologies of Samples A to D gradually evolved along the coordination and alcoholysis of EG with the Co(II) cation. More work is underway to determine the detailed structure of such metal alkoxides.

Morphological Diversification. We also found that the final morphology of the precursor is sensitive to the initial concentration of $Co(CH_3COO)_2 \cdot 4H_2O$ while starting from spheres. By controlling the initial concentration, the morphologies of synthesized architecture could be regulated. We investigated a series of samples with different $Co(CH_3COO)_2 \cdot 4H_2O$ concentrations while PVP concentrations remained the same. All the samples were taken from the solution after it was heated for 70 min to make sure that the phase transformation has completed. When the $Co(CH_3COO)_2 \cdot 4H_2O$ concentration was 6 mM, the sample was inclined to form flat nanoplates although some of them can also stack together. Figure 4a was a typical SEM image of this structure, similar to that in Figure 1d. When the concentration of $Co(CH_3COO)_2 \cdot 4H_2O$ was increased to 40 mM, the flat nanoplates tended to form distorted plates, which also piled up to form multilayer structure, as shown in Figure 4b. Figure 4c (Sample E) revealed that this tendency is further extended at 93 mM $Co(CH_3COO)_2 \cdot 4H_2O$. The plates were severely distorted and many layers of such distorted plates stack together, giving the whole structure a "cabbage-like" morphology. Finally, at the highest $Co(CH_3COO)_2 \cdot 4H_2O$ concentration of 160 mM, the self-assembled architecture became apparently micorspheres with an average diameter of 1.5 μm as shown in Figure 4d. Yet, close examination of the SEM images revealed that the surfaces of the spheres were not smooth. They seemed rather to be composite structures consisting of small distorted plates, which make the sphere look like a florescent chrysanthemum. It is noteworthy that the existence of PVP apparently had no significant impact on the formation of different morphologies, but it could improve the uniformity of the final architecture (Figure 5).

Further investigation is carried out by SEM to reveal the organization of such self-assembled complicated structures. A SEM image of Sample E was acquired on a tilted sample holder (Figure 6). The majority of its component was semiconvex in the opposite sides. The inset in Figure 6a was a high-magnification SEM image for the surface morphology, which showed the cabbage-like shape. Different fragments could also be observed in this sample and would be helpful for understand-

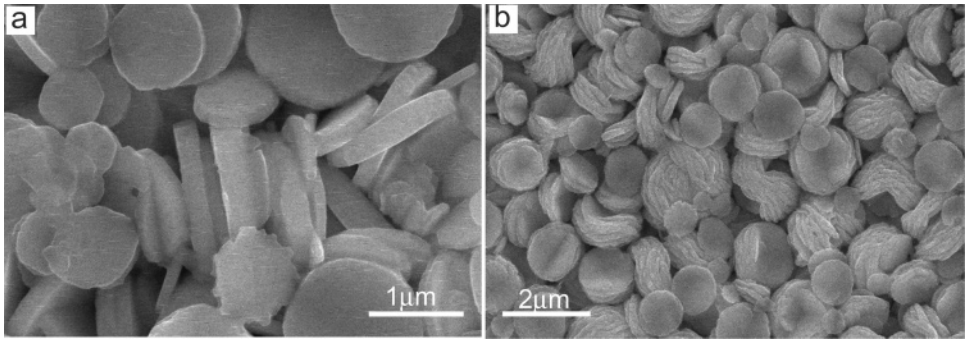

Figure 5. SEM pictures for samples without PVP while the concentrations of $Co(CH_3COO)_2 \cdot 4H_2O$ are varied: (a) 6 and (b) 93 mM.

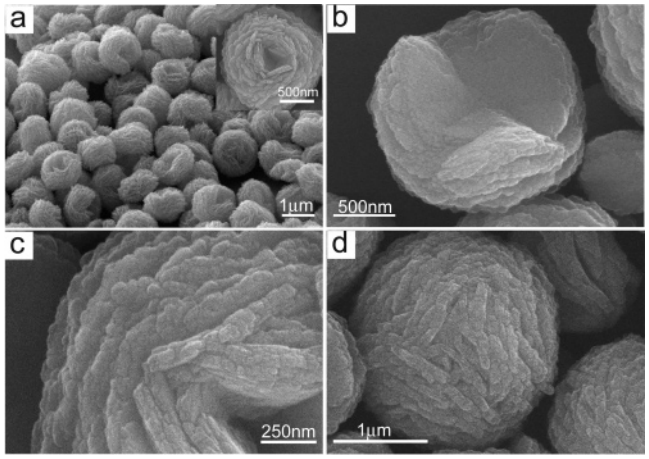

Figure 6. (a) SEM images of Sample E. The inset shows a high-magnification SEM image of the surface morphology. (b−d) SEM images of different pieces in Sample E.

ing the organizing manner. Instead of piling up to form a column,[21,29] the nanoplates tended to wrinkle up and form the notched template for further development, and then the following crystal growth was confined within the concave portion on both sides of the template thus developing a semiconvex superstructure (Figure 6b). A close examination of the rims (Figure 6c) showed a layer-by-layer growth style. The inside layer gradually curved and filled the concave portion formed by the template. Each side of the cabbage-like precursor was self-assembled by such well-regulated nanoplates. The final shape of the cabbage was determined by their stack efficiency. Spherical microspheres could also be sporadically found due to the total filling of the concave part (Figure 6d).

Growth Mechanism. The growth mechanism of nanocrystals remained an open question despite the great achievements in the preparations and applications of nanocrystals.[30] In our experiments, the time-dependent result was consistent with the process called kinetically driven crystallization, which usually includes an initial amorphous phase.[3] Such a phase was usually the result of supersaturation and fast nucleation at the initial stage. This phase was unstable and was susceptible to slow phase transformation.[3,31,32]Along with the gradual coordination and alcoholysis of EG with Co(II), a dissolution−renucleation process for amorphous spheres took place and the more stable crystalline phase emerged. The influence of concentration on the final morphologies revealed a hybrid mechanism for crystal growth.[33,34] At low concentration limit, there were a limited number of nucleation centers for slow crystal growth as the crystallization was diffusion controlled, and then the gradual attachment of constituent species onto the formed particles can form anisotropic plates.[33,34] For a medium concentration, there were many nucleation centers, and crystals grew faster. The existence of a large number of nucleation centers prevented a single nucleation center from growing too large and a curved structure could form.[34−37] The following growth took a layer-by-layer style so that a hierarchically self-assembled structure was developed. At a high concentration limit, the aggregation mechanism would be dominant in crystal growth and it finally led to isotropic microspheres as shown in Figure 4d.[33,34] The probable scheme for the evolution of the whole process with different morphologies is proposed as Figure 7.

Co_3O_4 Preparation and Characterization. After the preparation of the precursors, we investigated the effect of calcination on the crystallization and morphology of the samples. The subsequent calcination at 500 °C for 2 h had no noticeable effect on the morphology of these cobalt oxide precursors. The above-mentioned morphologies such as nanospheres, nanoplates, and stacked plates can basically be retained. Figure 8a showed a representative SEM image of the calcined Sample E, showing the preservation of the microspherical superstructures. Figure 8b shows a wide-angle XRD pattern of this calcined sample, which can be indexed as the cubic symmetry of Co_3O_4 (JCPDS card no. 78-1969), demonstrating the existence of crystalline Co_3O_4 through calcination. The TEM image in Figure 8c was in good agreement with the morphology as presented in the SEM picture. The high-magnification TEM image in Figure 8d revealed that the surface consists of nanocrystallites less than 20 nm in size and thus makes the sample porous. A high-resolution TEM (HRTEM) image taken from the nanoparticle is shown in the inset of Figure 8d. The lattice fringes are clearly visible with a spacing of 0.240 nm, which is in a good agreement with the spacing of the (311) planes of Co_3O_4. The Brunauer−Emmett−Teller (BET) gas sorptometry measurement showed that it was porous with the specific surface area of 36 m^2/g (Figure 9).

Sensing Performance. Intrigued by the hierarchical structure and the porosity of the synthesized Co_3O_4, we expected that this semiconductor oxide would be advantageous for sensor applications. A sensor based on the Co_3O_4 nanostructured material was fabricated. As a typical measurement, the sensor's sensitivity to alcohol was tested. Figure 10 presents an alcohol-sensing curve obtained from the calcined Sample E with a working temperature of 300 °C. The synthesized Co_3O_4 shows great sensitivity (>8) and reversibility to 50 ppm alcohol. As a comparison, the commercial breath analyzer has a low detection limit of 200 ppm. A recently reported Co_3O_4 nanotube synthesized by a porous-alumina-template method showed sensitivity around 3.[12] The sensor curve showed on and off characterization upon introduction and removing of alcohol with the response and recovery time being less than 10 s. The responses were very stable and could be repeated more than 10 times without major changes. With regard to practical use, the selectivity of the sensor was also a concern. Therefore, the selective sensitivity

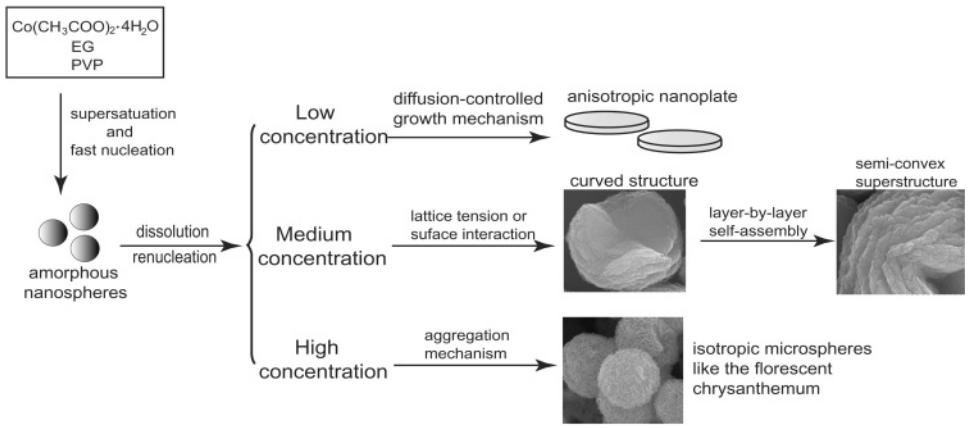

Figure 7. Schematic illustration of the morphology evolution of cobalt precursors

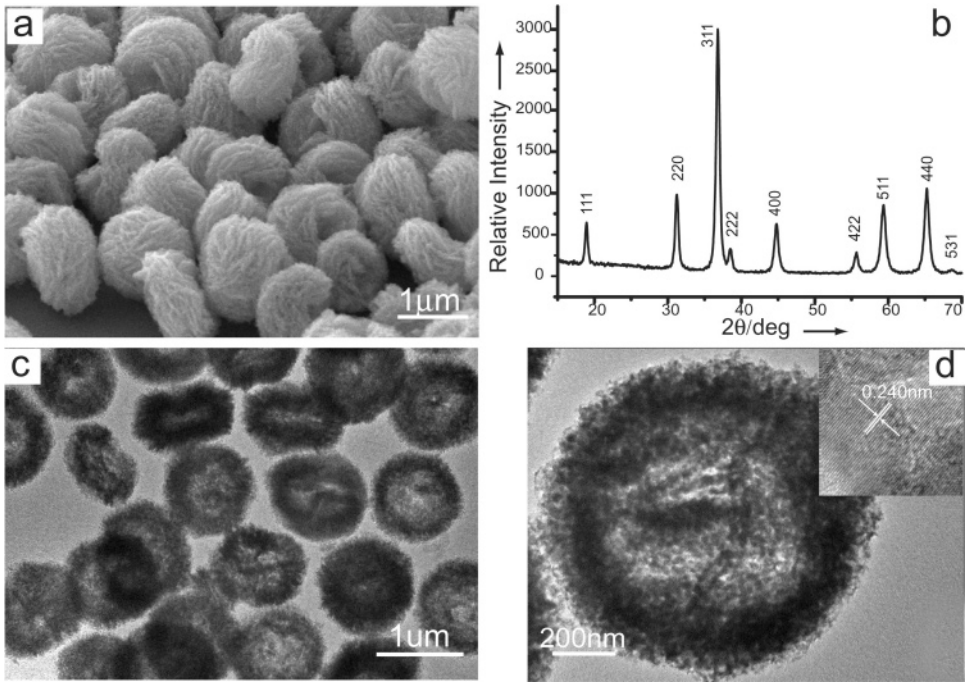

Figure 8. (a) SEM image, (b) XRD pattern, and (c) low- and (d) high-magnification TEM images of Co_3O_4 from the calcinations of Sample E. The inset in panel d is a high-resolution TEM (HRTEM) picture taken from the nanoparticle on the surface of the semiconvex structure.

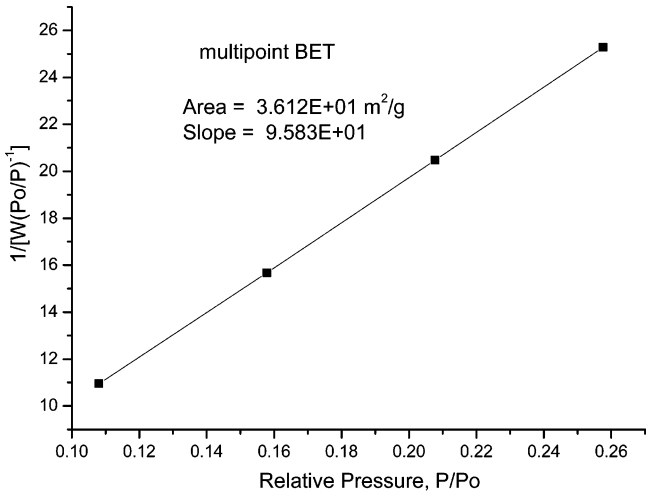

Figure 9. The multipoint BET measurement for calcinated Sample E. The specific surface area was calculated to be 3.612 × 10 m^2/g.

of the sensor to CO was tested as an example. It showed that the sensor was insensitive to 50 ppm CO and the resistance change was still at a much lower level even for 1000 ppm CO.

As a p-type oxide, the sensor mechanism was mainly due to the surface conductivity modulation by the adsorption and desorption of gas molecules.[28,38] For the Co_3O_4 sensor described here, we believe that the high performance can be attributed to the intrinsically higher order architectures with embedded structure across multiple length scales. The small grain size of less than 20 nm means that a large fraction of the atoms are present on the surface so that the surface property becomes paramount. Furthermore, the special semiconvex architecture might help the diffusion of the adsorbed species. The inside of the architecture also could be exposed to the gas molecules because of the porous structure. The well-organized nanostructure has attracted great interest for advanced functional materials and here we presented an example of its advantages over traditional bulk materials.

Conclusion

In summary, we have developed a polyol process to synthesize Co_3O_4 with a highly ordered superstructure. The morphol-

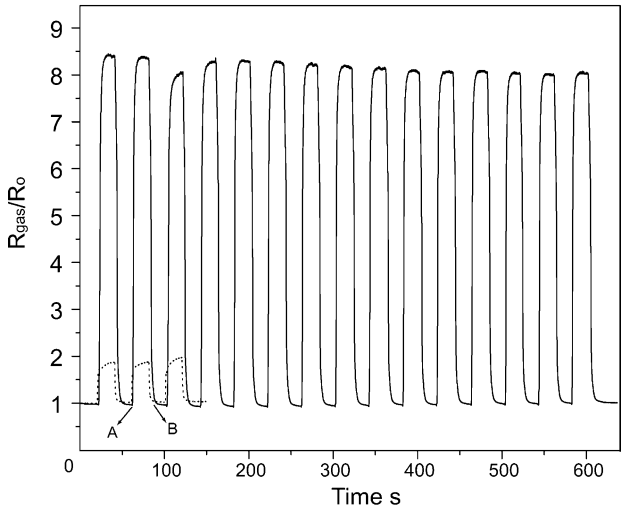

Figure 10. The alcohol sensing curve in a Co_3O_4-based sensor at 300 °C. The solid line is the response to 50 ppm alcohol and the dash line is to 1000 ppm CO, showing the selectivity of the sensor. The sensor is exposed to alcohol vapor or CO at A and for 20 s, then it is switched to dry air at B. The gas sensitivity is defined as the resistance ratio of R_{gas} to R_o, where R_{gas} and R_o are the electrical resistance for the sensor in alcohol or CO and in air, respectively.

ogies of the product were readily tunable by changing the concentration of $Co(CH_3COO)_2 \cdot 4H_2O$. The products showed various shapes from simple nanoplates to well-organized cabbage-like structures, and then to microspherical composites. The growth kinetics of such a process was also studied. The prepared Co_3O_4 exhibited good sensitivity, remarkable selectivity, and high stability as an alcohol sensor.

Acknowledgment. This work was supported by the National Natural Science Foundation of China (Nos. 20121301, 20520140277, and 20575070) and the National Key Project on Basic Research (Grants G2000077501 and 2002CCA03100). The Chinese Academy of Sciences is gratefully acknowledged. A.-M.C. thanks Prof. Chun-Li Bai for his supervision.

References and Notes

(1) Iijima, S. *Nature* **1991**, *354*, 56.
(2) Pai, R. A.; Humayun, R.; Schulberg, M. T.; Sengupta, A.; Sun, J. N.; Watkins, J. J. *Science* **2004**, *303*, 507.
(3) Colfen, H.; Mann, S. *Angew. Chem., Int. Ed.* **2003**, *42*, 2350.
(4) Corma, A.; Rey, F.; Rius, J.; Sabater, M. J.; Valencia, S. *Nature* **2004**, *431*, 287.
(5) Lu, W. G.; Gao, P. X.; Bin Jian, W.; Wang, Z. L.; Fang, J. Y. *J. Am. Chem. Soc.* **2004**, *126*, 14816.
(6) Gong, J. R.; Zhao, J. L.; Lei, S. B.; Wan, L. J.; Bo, Z. S.; Fan, X. L.; Bai, C. L. *Langmuir* **2003**, *19*, 10128.
(7) Fan, H. Y.; Yang, K.; Boye, D. M.; Sigmon, T.; Malloy, K. J.; Xu, H. F.; Lopez, G. P.; Brinker, C. J. *Science* **2004**, *304*, 567.
(8) Schreiber, F. *Prog. Surf. Sci.* **2000**, *65*, 151.
(9) Wang, S. D.; Dong, X.; Lee, C. S.; Lee, S. T. *J. Phys. Chem. B* **2004**, *108*, 1529.
(10) Breen, T. L.; Tien, J.; Oliver, S. R. J.; Hadzic, T.; Whitesides, G. M. *Science* **1999**, *284*, 948.
(11) Cao, A. M.; Hu, J. S.; Liang, H. P.; Wan, L. J. *Angew. Chem., Int. Ed.* **2005**, *44*, 4391.
(12) Li, W. Y.; Xu, L. N.; Chen, J. *Adv. Funct. Mater.* **2005**, *15*, 851.
(13) Wollenstein, J.; Burgmair, M.; Plescher, G.; Sulima, T.; Hildenbrand, J.; Bottner, H.; Eisele, I. *Sens. Actuators, B* **2003**, *93*, 442.
(14) Jana, N. R.; Chen, Y. F.; Peng, X. G. *Chem. Mater.* **2004**, *16*, 3931.
(15) Nethravathi, C.; Sen, S.; Ravishankar, N.; Rajamathi, M.; Pietzonka, C.; Harbrecht, B. *J. Phys. Chem. B* **2005**, *109*, 11468.
(16) Nethravathi, C.; Sen, S.; Ravishankar, N.; Rajamathi, M.; Pietzonka, C.; Harbrecht, B. *J. Phys. Chem. B* **2005**, *109*, 11468.
(17) He, T.; Chen, D. R.; Jiao, X. L.; Xu, Y. Y.; Gu, Y. X. *Langmuir* **2004**, *20*, 8404.
(18) Wang, Y. Q.; Yang, C. M.; Schmidt, W.; Spliethoff, B.; Bill, E.; Schuth, F. *Adv. Mater.* **2005**, *17*, 53.
(19) Lakshmi, B. B.; Patrissi, C. J.; Martin, C. R. *Chem. Mater.* **1997**, *9*, 2544.
(20) Feng, J.; Zeng, H. C. *Chem. Mater.* **2003**, *15*, 2829.
(21) Tian, Z. R. R.; Voigt, J. A.; Liu, J.; McKenzie, B.; McDermott, M. J.; Rodriguez, M. A.; Konishi, H.; Xu, H. F. *Nat. Mater.* **2003**, *2*, 821.
(22) Hu, J. S.; Ren, L. L.; Guo, Y. G.; Liang, H. P.; Cao, A. M.; Wan, L. J.; Bai, C. L. *Angew. Chem., Int. Ed.* **2005**, *44*, 1269.
(23) Larcher, D.; Sudant, G.; Patrice, R.; Tarascon, J. M. *Chem. Mater.* **2003**, *15*, 3543.
(24) Chakroune, N.; Viau, G.; Ammar, S.; Jouini, N.; Gredin, P.; Vaulay, M. J.; Fievet, F. *New J. Chem.* **2005**, *29*, 355.
(25) Feldmann, C.; Jungk, H. O. *Angew. Chem., Int. Ed.* **2001**, *40*, 359.
(26) Feldmann, C. *Adv. Funct. Mater.* **2003**, *13*, 101.
(27) Jiang, X. C.; Wang, Y. L.; Herricks, T.; Xia, Y. N. *J. Mater. Chem.* **2004**, *14*, 695.
(28) Wang, Y. L.; Jiang, X. C.; Xia, Y. N. *J. Am. Chem. Soc.* **2003**, *125*, 16176.
(29) Tian, Z. R. R.; Voigt, J. A.; Liu, J.; McKenzie, B.; McDermott, M. J. *J. Am. Chem. Soc.* **2002**, *124*, 12954.
(30) Zhang, J.; Wang, Z.-L.; Liu, J.; Chen, S.; Liu, G.-Y. *Self-Assembled Nanostructures*; Kluwer Academic/Plenum Publishers: New York, 2003.
(31) Testino, A.; Buscaglia, M. T.; Buscaglia, V.; Viviani, M.; Bottino, C.; Nanni, P. *Chem. Mater.* **2004**, *16*, 1536.
(32) Loste, E.; Wilson, R. M.; Seshadri, R.; Meldrum, F. C. *J. Cryst. Growth* **2003**, *254*, 206.
(33) LaMer, V. K.; Dinegar, R. H. *J. Am. Chem. Soc.* **1950**, *72*, 4847.
(34) Suber, L.; Sondi, I.; Matijevic, E.; Goia, D. V. *J. Colloid Interface Sci.* **2005**, *288*, 489.
(35) Park, J.; Privman, V.; Matijevic, E. *J. Phys. Chem. B* **2001**, *105*, 11630.
(36) Perez-Maqueda, L. A.; Wang, L.; Matijevic, E. *Langmuir* **1998**, *14*, 4397.
(37) Wang, L.; Sondi, I.; Matijevic, E. *J. Colloid Interface Sci.* **1999**, *218*, 545.
(38) Liu, J. F.; Wang, X.; Peng, Q.; Li, Y. D. *Adv. Mater.* **2005**, *17*, 764.